RF-MEMS switches for a full control of the propagating modes in uniplanar microwave circuits and their application to reconfigurable multimodal microwave filters

A Contreras[1], J. Casals[2], L Pradell[1], M. Ribó[3], J Heredia[1], F. Giacomozzi[4], B. Margesin[4]

[1]Department of Signal Theory and Communications, Technical University of Catalonia (UPC), 08034 Barcelona, Catalonia, Spain. [2]Mechanical Engineering Department, Technical University of Catalonia (UPC), 08034 Barcelona, Catalonia, Spain [3]Electronics and Telecommunications Department, La Salle – Ramon Llull University (URL) Barcelona, Catalonia, Spain. [4]Fondazione Bruno Kessler (FBK), Via Sommarive 18, 38123 Trento, Italy

E-mail: pradell@tsc.upc.edu

Abstract. In this paper, new RF-MEMS switch configurations are proposed to enable control of the propagating (even and odd) modes in multimodal CPW transmission structures. Specifically, a switchable air bridge (a switchable short-circuit for the CPW odd mode) and switchable asymmetric shunt impedances (for transferring energy between modes) are studied and implemented using bridge-type and cantilever-type ohmic-contact switches, respectively. The switchable air bridge is based in a novel double ohmic-contact bridge-type structure. Optimized-shape suspension configurations, namely folded-beam or diagonal-beam for bridge-type switches, and straight-shaped or semicircular-shaped for cantilever-type switches, are used to obtain robust structures against fabrication-stress gradients. The switches are modelled using a coupled-field 3D finite-element mechanical analysis showing a low to moderate pull-in voltage. The fabricated switches are experimentally characterized using *S*-parameter and DC measurements. The measured pull-in voltages agree well with the simulated values. From *S*-parameter measurements, an electrical model with a very good agreement for both switch states (ON and OFF) has been obtained. The model is used in the design of reconfigurable CPW multimodal microwave filters.

1. Introduction

Tunable and reconfigurable RF and microwave devices will play an important role in the development of next-generation multi-band communication systems, because they can reduce dramatically their overall size, weight and power consumption. To provide reconfiguration, the use of RF-MEMS switches with electrostatic actuation has demonstrated superior performance (in comparison to semiconductor switches) in terms of linearity and extremely low power consumption (Rebeiz et al. 2009; Lucyszyn 2004), leading to circuits which are compact and energy-efficient. Most of the MEMS-reconfigurable RF and microwave devices available in the literature are implemented using either *microstrip* transmission lines or uniplanar transmission lines such as *coplanar waveguides* (*CPW*), the *coplanar striplines* (*CPS*) and *slotlines* (Wolff 2006) (Fig. 1). In contrast to microstrip lines, uniplanar transmission lines are characterized by having all line metallization on the same plane, and thus shunt components do not require holes (vias) through the substrate. Therefore uniplanar transmission lines offer excellent reconfiguration capabilities because either series or shunt components, such as ohmic-contact (or capacitive-contact) RF-MEMS switches or varactors, can be easily mounted on them. A distinct feature of the CPW with respect to CPS and slotline is the fact that it is a *multimodal* transmission line, which can simultaneously propagate two fundamental modes, the even mode (Fig. 1(c)) and the odd mode (Fig. 1(d)). The presence of two fundamental modes in the same CPW section allows the design of innovative compact reconfigurable microwave circuits since more circuit functionality can be assembled in less area. This *multimodal approach* has already been applied by the authors to the design of 90º-hybrids (Llamas et al. 2009) compact bandpass filters (Contreras et al. 2013) and also RF-MEMS enabled reconfigurable devices, such as phase switches (Llamas et al. 2010; 2011) and bandpass filters with reconfiguration of center-

frequency (Contreras et al. 2014) or bandwidth (Contreras et al. 2013). RF-MEMS switches offer a simple yet effective solution to provide reconfiguration in multimodal circuits since these require a selective control of each CPW mode (even (Llamas et al. 2010; 2011) and odd (Contreras et al. 2013; 2014), which can be accomplished only in particular cases using semiconductor switches (Contreras et al. 2011). Uniplanar topologies using a *single-mode* (even mode only) classical design approach have also been extensively reported in the literature to implement a variety of MEMS-reconfigurable RF and microwave devices, in particular phase shifters (Van Caekenberghe et al. 2008) and filters (Nordquist et al. 2004; Fourn et al. 2003; Ocera et al. 2006; Pothier et al. 2005; Yuk et al. 2012; Park et al. 2006; Nordquist et al. 2005; Reines eut al. 2008; Entesari et al. 2005; Scarbrough et al. 2009).

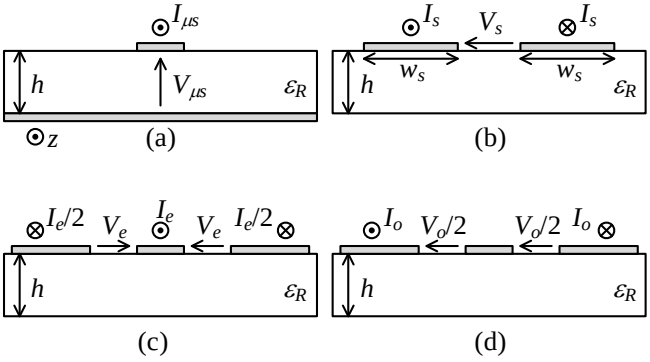

Fig. 1 Cross sections of several types of transmission lines patterned on a dielectric substrate of height h and dielectric relative permittivity ε_R (metallizations are shown in grey) with the definitions of the voltages and currents of their propagating modes. (a) Microstrip transmission line propagating the microstrip (μs) mode. (b) Slotline (wide w_s) or CPS (narrow w_s) propagating the slotline/CPS (s) mode. (c) CPW propagating its even (e) mode. (d) CPW propagating its odd (o) mode.

Concerning the RF-MEMS mechanical topologies required in microwave reconfigurable circuits they typically include clamped-clamped bridges or cantilever switches (either ohmic or capacitive), with different type of suspensions such as straight-beam (Contreras et al. 2013; Fedder 1994; Persano et al. 2016) and folded-beam (Contreras et al. 2012; 2014; Fedder 1994; Peroulis et al. 2003, Kim et al. 2014; Kim et al. 2009; Lakshmi et al. 2016). The type of suspension influences the fabrication residual stress of the MEMS membrane, a critical parameter to meet the desired ON/OFF capacitance ratio in capacitive switches, the contact resistance in ohmic switches, and the actuation voltages (Peroulis et al. 2003; Mahameed et al. 2010; Philippine et al. 2013; Persano et al. 2016; Kim et al. 2009; Lakshmi et al. 2016), which in turn determine the microwave behavior (central frequency, bandwidth) of frequency-reconfigurable filters. A solution to this problem is the use of RF-MEMS switched capacitors to obtain precise frequency shifts (Pothier et al 2005; Nadaud et al. 2016). The fabrication residual stress can be reduced either by improving the geometry and the structural switch design (Mahameed et al. 2010; Philippine et al. 2013; Patel et al. 2012; Zaireie et al. 2013; Yang et al. 2015), since these determine their stiffness and therefore actuation voltage and reliability, or utilizing particular materials, and therefore a special dedicated fabrication process (Palego et al. 2009, Ke et al. 2013, Sterner et al. 2008). In (Patel et al. 2012) a crab-leg beam geometry is used to achieve a highly reliable switch, but with a high actuation voltage (80–90 V). In (Zaireie et al. 2013) a modification of this type of suspension was proposed, where one part of the suspensions had an in-plane angle to decrease the influence of residual stresses. In (Mahameed et al. 2010), an in-plane chevron-type switch was presented; this structure released the residual stresses and therefore it was temperature/stress-stable when actuated out of plane. In (Philippine et al. 2013) a topology optimization was used to propose stress-insensitive geometries. The aforementioned structures had been fabricated out of different metal layers for low signal loss. However, their different thermal expansion coefficients (larger than those of substrate materials) generate residual stresses during fabrication and performance variability under temperature gradients.

In this paper, new RF-MEMS switch configurations which enable a selective control of the even and odd modes in CPW-based structures, for compact, reconfigurable multimodal microwave circuits are proposed, and the procedure to transfer energy from the even mode to the odd mode (and vice-versa) is discussed in detail through a multimodal circuit approach. To this end, standard cantilever ohmic-contact switches (*switchable asymmetric shunt impedances*) and a novel ohmic-contact switch design, are used.

The latter was first introduced in (Contreras et al. 2012) and consists of a bridge with two ohmic contacts (one at each end of the membrane) which behaves as a switchable short-circuit for the CPW odd mode (*switchable air bridge*) that does not affect the propagation of the even mode. Using two ohmic contacts keeps the switch structure symmetric (which is required in order not to affect the propagating CPW even mode) with the additional advantage of introducing redundancy in case one contact fails. Furthermore, a combination of optimized-shape suspensions (folded beam as in (Contreras et al. 2012), and diagonal beam) and a reinforced membrane is used, resulting in a robust structure against either positive or negative stress gradients. To perform the mechanical evaluation of the different devices, a finite-element analysis has been developed and the simulated pull-in voltage and residual stress have been validated through experimental measurements. The RF-MEMS devices are used in reconfigurable multimodal CPW microwave resonators and filters, for which multimodal equivalent circuits including the RF-MEMS switch effects are proposed. The filter reconfiguration capability includes central frequency (keeping a constant fractional bandwidth FBW) and bandwidth (keeping a constant central frequency). The proposed RF-MEMS switches and filters which integrate the switches are fabricated using the eight-mask surface micromachining process from FBK (Giacomozzi et al. 2011) and experimentally validated. The measured switches behavior shows a good agreement with mechanical and electromagnetic simulations. The filters performance also agrees well with the multimodal circuit thus validating the proposed configurations for controlling the propagating (even and odd) modes.

2. RF-MEMS switch designs

In this section the proposed MEMS-switch configurations for the control of the propagating modes in a CPW multimodal environment will be presented. Next the proposed switches will be described in detail.

2.1. RF-MEMS switches for controlling the CPW modes

In multimodal CPW designs, even and odd mode waves performing different tasks coexist in the same circuit area. This results in circuit size reduction and reconfiguration capability if the modes are controlled by means of low-loss high-isolation switches or switched capacitors.

To understand how this control can be achieved, consider the CPW configurations of Fig. 2. Fig. 2(a) shows a CPW with a series switch in the center conductor. When it is ON, nothing happens: the even and odd modes propagate as in a conventional CPW. When it is OFF, it blocks the propagation of the even mode since it forces $I_e = 0$ but, since there is no current on the center conductor for the odd mode, it has no effect on it. Therefore, the multimodal model for the circuit (a model that splits each mode present at the transition in a different ideal transmission line) is that of Fig. 2(b), where Z_{0e} and Z_{0o} are respectively the characteristic impedances of the even and odd mode. The model rigorously takes into account that an even-mode wave that enters into the circuit is reflected back by the switch in OFF, while an odd-mode wave propagates undisturbed between the input and output port. Thus, the propagation of the even mode can be controlled independently of that of the odd mode. Fig. 2(c) shows a CPW with a switch that connects the lateral ground planes (a *switchable air bridge* (SAB)). When it is OFF, nothing happens, but when it is ON, if forces the same potential at both lateral conductors and therefore short-circuits the odd mode ($V_o = 0$). Since for the even mode the lateral conductors are equipotential the even mode is not affected. Therefore the multimodal model of the circuit is that of Fig. 2(d). This way, the propagation of the odd mode can be controlled independently of that of the even mode. Fig. 2(e) shows a symmetric capacitor (which could be switchable if required) connected to a CPW. Since the field configurations are different for the even and odd modes, it will affect them in a different way, as shown in Fig. 2(f). The building block of a CPW multimodal circuit contains structures that controllably transfer energy from one mode to the other, such as a switch placed over one of the CPW slots (a *switchable asymmetric shunt impedance*) shown in Fig. 2(g). When it is OFF, nothing happens. When it is ON, a modal interaction takes place that can be described by the multimodal model in (Ribó et al. 1999). Therefore its multimodal model is that of Fig. 2(h). As can be seen, now the even mode and the odd mode interact electrically through the ideal transformer. Thus, a switchable asymmetric shunt impedance constitutes a way to control the generation of one mode from the other.

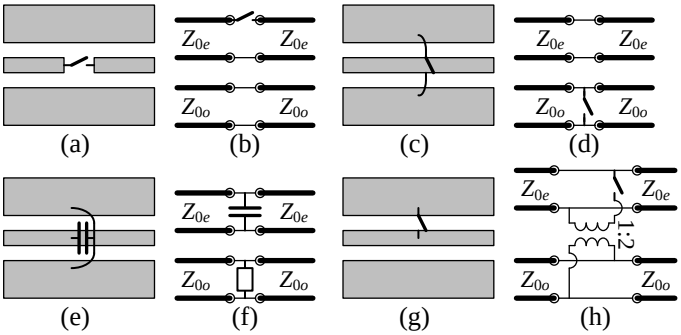

Fig. 2 (a) Gap in a CPW. (b) Multimodal circuit model for the gap in (a). (c) Air bridge in a CPW. (d) Multimodal circuit model for the air bridge in (c). (e) Capacitor (which can be fixed, variable or switched) in a CPW. (f) Multimodal circuit model for the capacitor in (e). (g) Asymmetric shunt short-circuit in a slot of a CPW. (h) Multimodal circuit model for the asymmetric shunt short-circuit in (g).

In order to see how the above strategies can lead to compact reconfigurable circuits consider the example of Fig. 3(a), wherein a CPW section intended for connecting two other circuits by means of the even mode is modified to include two conventional air bridges, two SABs and a switchable asymmetric shunt impedance. Its circuit model, obtained by connecting those in Fig. 2, is shown in Fig. 3(b). When all the switches are OFF, since the even mode is not affected by air bridges, the CPW section performs its original task. When the switchable asymmetric shunt impedance is ON, part of the energy of the even mode is transferred to the odd mode, which will propagate until it is short-circuited by the air bridges. Therefore a load (a shunt odd-mode resonator) has been embedded into the original (even-mode) CPW section without increasing the circuit size. This odd mode resonator will completely block the propagation of even mode signals (from A to B in Fig. 3(b)) at the frequency wherein its length is $\lambda_o/2$, where λ_o is the wavelength of the odd mode. To reconfigure the blocked frequency, the SABs must be turned ON, in order to modify the odd-mode resonator length.

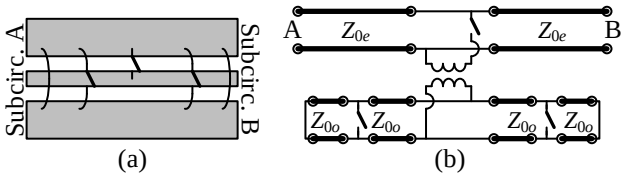

Fig. 3 (a) Switchable and reconfigurable odd-mode parallel $\lambda_o/2$ resonator embedded in a CPW section. (b) Equivalent multimodal circuit.

2.2. Cantilever-type switches for switchable asymmetric shunt impedances

Fig. 4(a) shows a schematic top view of the proposed structure for an ohmic-contact RF-MEMS cantilever-type switch with electrostatic actuation that can implement a switchable asymmetric shunt impedance (Fig. 2(g)). The cantilever is anchored to one of the lateral ground planes. An actuation electrode is placed underneath the cantilever, in the CPW slot. When a DC-actuation voltage equal or higher than the pull-in voltage (V_{pull_in}) is applied between the electrode and the cantilever, the cantilever collapses with the CPW center conductor closing the switch (ON state), as shown in Fig. 4(b). The switch features either straight-shaped suspension (STS) or semicircular-shaped suspension (SSS) (shown in Fig. 4(a)) optimized to minimize the membrane deformation induced by fabrication residual stresses. Under a perpendicular applied force, the SSS will combine torsional and flexural bending. Torsional deflection provides robustness toward residual stress. In addition to the SSS, a reinforced membrane can be used, as explained in Section 3, leading to a robust structure which is quite stable against either positive or negative fabrication residual stress gradients. This cantilever-type switch is applied to microwave reconfigurable bandwidth filters as explained in Section 5.

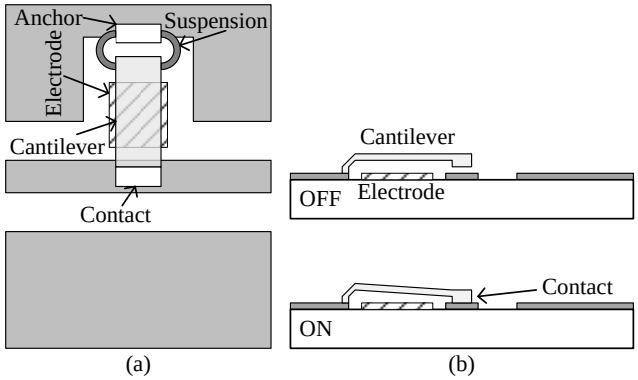

Fig. 4 Cantilever-type switch. (a) Schematic top-view of the SSS configuration. (b) Device cross-section showing ON and OFF states.

2.3. Bridge-type switches

Fig. 5(a) shows a schematic top view of the proposed structure for RF-MEMS ohmic-contact bridge-type switches with electrostatic actuation that implement a SAB (Fig. 2(c)) in a CPW section. The membrane is anchored to isolated islands placed in either CPW slot. Two electrodes are placed symmetrically underneath the bridge in either slot of the CPW. Two ohmic contacts are defined on the top and bottom edges of the bridge, respectively, which connect the two ground planes when the switch in ON, as shown in the cross-section of Fig. 5(c). The bridge has a center window in order to minimize the unwanted capacitance between the membrane and the center conductor of the CPW. This spurious capacitance would affect the even-mode propagation when the SAB is ON in a way similar to that of Fig. 2(e)–(f), and would reduce the capability of a SAB to exclusively control the propagation of the odd mode. The switches feature either folded-beam suspension (FBS) or diagonal-beam suspension (DBS). These suspensions were chosen to compensate for intrinsic residual stresses induced by the fabrication process and to provide a good trade-off between the spring constant value and the spacing between membrane and electrodes to obtain a moderate actuation voltage. In the case of FBS, the two arms of the folded beams feature equal (or very similar) lengths. As for DBS, the V-arm geometry cancels out the forces generated by the residual stress. It was found that the V arms should emerge from the body of the suspended membrane with an angle α that has been optimized to ensure a stable actuation. In addition to the suspension type (FBS or DBS), a reinforced membrane is used, as explained in Section 3, leading to a robust structure which is stable against either positive or negative fabrication residual stress gradients.

The same FBS/DBS structures can also be used to implement switched capacitors (Fig. 5(b)), in which case the membrane is anchored to the two lateral ground planes. The cross-section of Fig. 5(d) shows the behavior of the device in its ON and OFF states. The capacitive contact is implemented by sequential deposition of a thin dielectric layer on top of the central conductor and a thin floating metal layer (FLOMET) on top of the dielectric layer. This way a MIM switched-capacitor with a definite and constant high capacitance value in its ON state (C_{ON}) is defined, ensuring a repetitive value of C_{ON}, and thus a stable RF performance in ON state. In its OFF state (bridge in "up" position), the switched capacitor features a very low capacitance value (C_{OFF}) and behaves as a fixed air bridge with a negligible effect for the odd mode. Thus C_{ON} and the capacitance ratio C_{ON} / C_{OFF} are high enough, and the switched capacitor behaves as an even-mode switch (Fig. 2(e)).

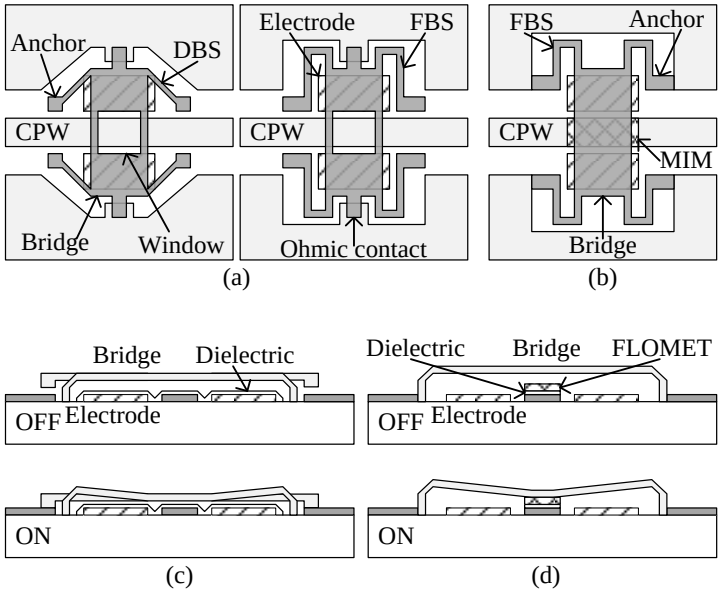

Fig. 5 Proposed switches. (a) Schematic top-views of FBS and DBS configurations for SABs showing the two ohmic-contacts. (b) Schematic top-view of a FSB configuration for a capacitive-contact switch implementing a (MIM) switched capacitor. (c) Cross-section of an ohmic-contact SAB, in ON and OFF states. (d) Cross-section of a capacitive-contact switch, in ON and OFF states.

3. RF-MEMS switch mechanical simulations and fabrication

In this section the fabrication process for the switches proposed in Section 2 will be described, the FEA mechanical simulations obtained from the ANSYS® Workbench ™ discussed, and the fabricated switches will be presented.

3.1. Fabrication process

The technology used for the fabrication of the RF-MEMS switches proposed in this paper consists of an integrated eight-mask surface-micro-machining process, developed by the MEMS group of FBK (Giacomozzi et al. 2011). This process was developed to produce high performant RF-MEMS-switch structures and other passive components for RF and microwave components based on CPW and microstrip transmission lines, for which very low losses both in metal and dielectric layers are required. The RF-MEMS devices are fabricated on low-loss substrates such as high-resistivity silicon (Hi_res Si), or quartz. Fig. 6 shows the fabrication process flow on silicon substrates. First, an insulating layer consisting of 1 μm of silicon oxide is grown by wet thermal oxidation. The DC-actuation pads and bias lines are defined by using a high-resistivity polysilicon layer with a thickness of 0.63 μm. To improve the contact resistance of the ohmic contacts, small dimples (typically of 4 μm × 4 μm) of polysilicon are realized in this same step, thus creating contact bumps that define exactly the number and position of contact points between the movable membrane and the *underpass* signal line. A 300-nm-thick insulating layer of SiO_2 is deposited by LPCVD (low-pressure chemical vapor deposition) using TEOS (tetraethyl orthosilicate). A second lithography step defines the opening for the contacts (Fig. 6(a)). A multi-metal layer (Ti/TiN/Al/Ti/TiN) is then deposited by sputtering and used as an underpass to connect signal lines under suspended structures (Fig. 6(b)). The thickness of the multi-metal underpass is the same as the polysilicon layer (0.63 μm) in order to avoid a lack of planarity in the movable membrane. Then a 100-nm-thick SiO_2 dielectric layer (low-temperature oxide, LTO) is deposited. The next lithography step defines the vias in the LTO. A 5-nm-Cr–150-nm-Au layer (Fig. 6(c)) is deposited by electron-beam gun to be used as floating metal (FLOMET) and to reduce the metal-gold resistance inside the vias. This 150-nm layer defines either MIM capacitors or ohmic contacts. For the fabrication of suspended movable membranes and air bridges, different thicknesses of photoresist sacrificial layer (spacer) can be used (Fig. 6(d)). The standard thickness is 3 μm, but thinner spacer layers (1.6 μm) are possible to achieve smaller actuation voltages. To define the metal layers of transmission lines (such as CPW) and the suspended membranes, two gold layers of different thicknesses can be deposited by electroplating. The movable bridges and cantilevers are manufactured using a 1.8-μm-thick gold layer (Fig. 6(e)), and a second 3.5-μm-thick superimposed gold layer (Fig. 6(f)) is deposited to define transmission lines and to have stiffer

parts of the membrane that move rigidly (reinforced membrane), while deformation is localized on thinner suspension spring legs. To release the suspended structures, the spacer is removed using oxygen plasma.

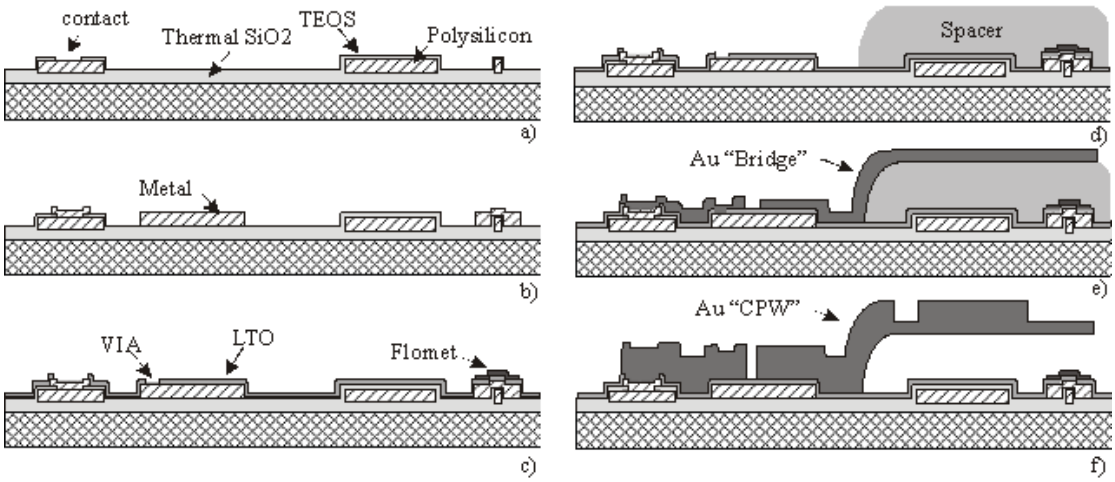

Fig. 6 Process flow for RF-MEMS switches from FBK (Giacomozzi et al. 2011). (a) Thermal oxidation; polysilicon and TEOS deposition and contact opening. (b) Metal deposition and patterning. (c) LTO deposition, vias opening and floating metal (FLOMET) deposition. (d) Spacer deposition. (e) Seed layer and first gold "bridge" electroplating. (f) Second gold "CPW" electroplating and release of suspended structures.

3.2. Mechanical simulations

In previous works analytical values for the effective stiffness of common suspensions types (i.e. straight-shaped (Young et al. 2012), semicircular-shaped (Wong et al. 2011) or FBS (Fedder 2004)) have been provided. However RF-switch manufacturing processes induce intrinsic residual stresses which modify the initial bridge shapes and therefore change the effective stiffness and increase the required actuation voltage *V*. A coupled-field 3D finite element analysis (FEA) using ANSYS® Workbench ™ is used here to take into account the residual stresses produced by the fabrication process on the reinforced membrane and the suspension. In ANSYS® Workbench ™ the dimensions of the RF MEMS switch can be parameterized, its 3D model is built and the physical properties of the materials of the switch are defined (table 1). After meshing the structure and defining the boundary conditions, the initial loads are applied. In this simulation the loads are the residual stresses, which are different in each structural layer, i.e. σ_2 = 58 MPa in the gold layer with a thickness t_2 = 1.8 μm and σ_1 = 62 MPa in the gold layer with a thickness t_1 = 3.5 μm, according to the membrane bi-layer structure (CPW and bridge layers) depicted in Fig. 6 (Mulloni et al. 2013). Fig. 7 shows the initial deformation of each of the different switches due to the residual stress. As expected some structures are more robust against stress. For instance, the SSS cantilever switch shows an initial deflection of 70 nm less than the STS cantilever. The DBS switch has a similar initial deformation compared to the FBS switch with suspensions of equal beam length but a higher spring constant, therefore an increased contact force. The FBS with suspensions of different beam length has a deflection due to stress of 40 nm more than the DBS and FBS with equal beam length.

Table 1. Material properties.

Symbol	Description	Value
σ	Residual stress (MPa) (Mulloni et al. 2013)	58–62
E	Young modulus (GPa) (Mulloni et al. 2013)	98.5±6
ρ	Density (kg/m^3)	19840

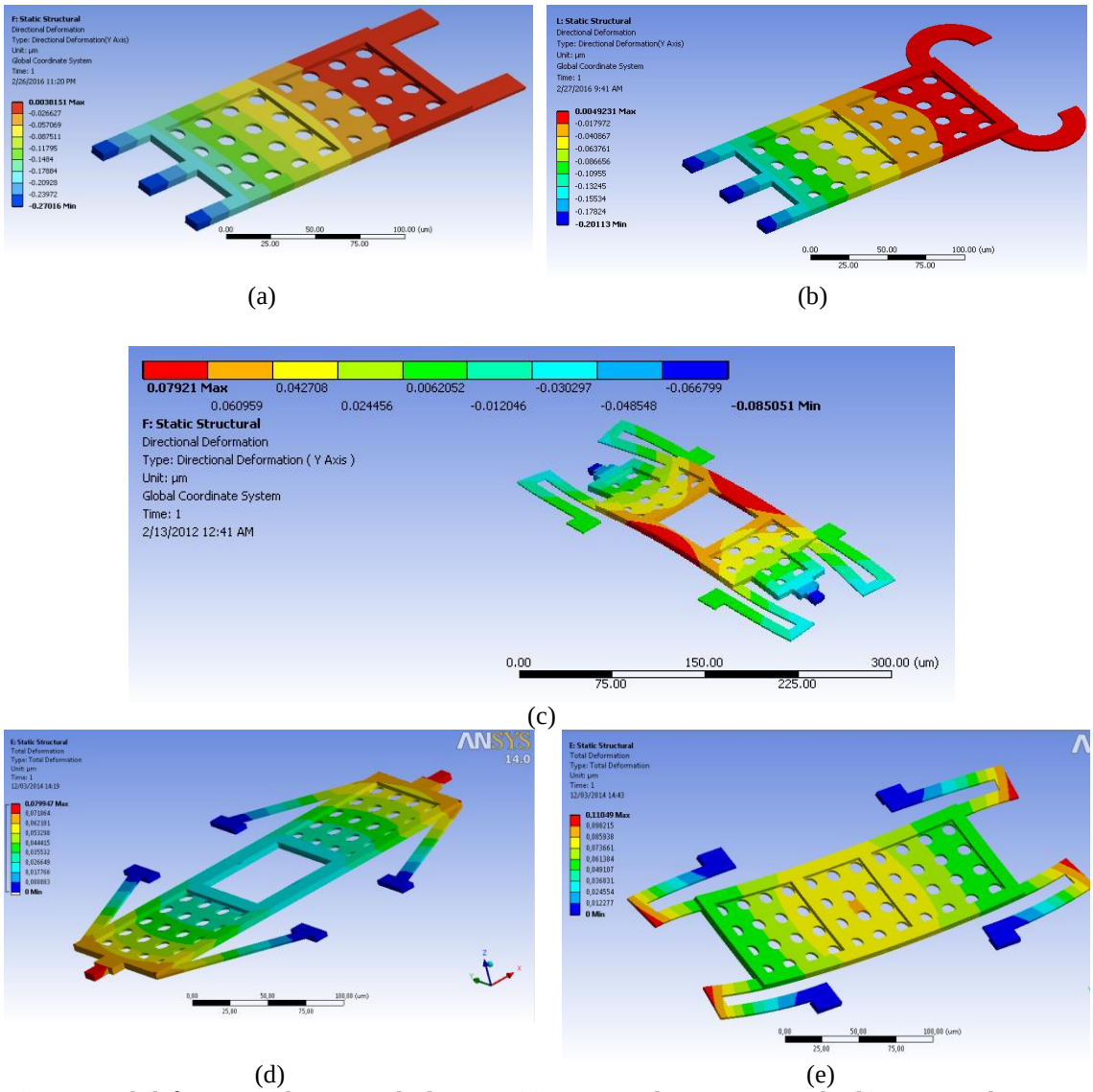

Fig. 7 Initial deformation due to residual stress. (a) STS cantilever-type switch. (b) SSS cantilever-type switch. (c) FBS bridge-type switch with suspensions of equal beam length. (d) DBS bridge-type switch. (e) FBS bridge-type switch with suspensions of different beam length (capacitive-contact).

The results from this simulation are then used as initial state in a coupled field simulation that uses EMTGEN macro to create an array of nonlinear, coupled, electromechanical transducer elements (TRANS126) that couples the electrostatic and structural domain. The EMTGEN macro creates the electrode to the appropriate distance (1.6 / 2.7 μm), depending on the thickness of the spacer. Table 2 in Section 3.3 lists the geometrical dimensions of the structures studied in Fig. 7 along with the simulated mechanical parameters (actuation voltage V_{pull_in}, spring constant k_{eff}, and mechanical resonant frequency) Fig. 8 shows the position of the switches once the pull-in voltage is applied. The bridge switches are more robust than the cantilever switches since the stiffness is much higher (around 40 N/m compared to 10 N/m), with a low-to-moderate pull-in voltage (≈ 15 V / 38 V compared to 8 V in cantilevers). From the three bridge configurations, the DBS has a similar behavior to residual stress compared to FBS with equal beam length, but the DBS has more bridge area as well as bottom electrode area, therefore it can create a more compact design for the same actuation characteristics.

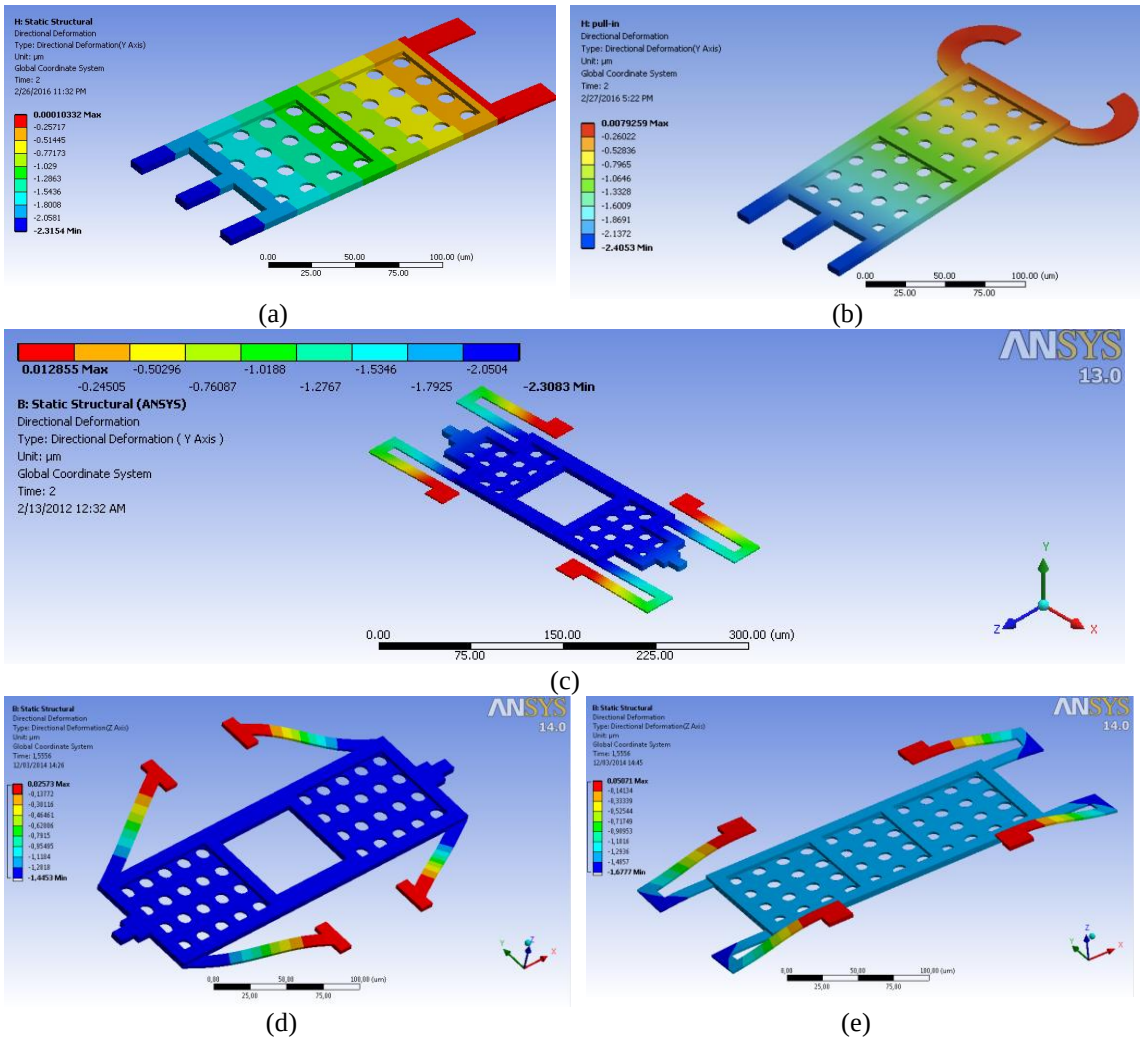

Fig. 8 Contact achieved once the V_{pull_in} is applied (same switches as in Fig. 7).

3.3. Fabricated devices

The different MEMS switch configurations discussed in Section 2 (depicted in Fig. 4 and Fig. 5) have been implemented using the FBK technology described above. They all are manufactured using a 1.8-μm-thick gold layer and reinforced using a stiffening 3.5-μm-thick gold frame. The distance between the movable membrane and the bottom electrode is either 1.6 μm or 2.7 μm. Two low-loss substrates, 5-kΩ·cm Hi_res Si (ε_r = 11.9 and thickness h = 200 μm) and quartz (ε_r = 3.8) have been used. Fig. 9 and Fig. 15(b) show pictures of the fabricated switches and Table 2 lists the device geometrical dimensions. The DC-bias is applied to the device electrodes by contacting two pads which are connected to two multi-metal underpass lines under the suspended structures (narrow lines in light brown in Fig. 9). The CPW slot width is 20 μm and the central conductor width is 50 μm (FBS), 35 μm (DBS) and 60 μm (STS and SSS). Fig. 10 shows an optical-profiler image and a plot of the surface profile of one of the fabricated devices. As can be seen, the membrane is almost flat. There is a very small negative stress gradient, which has little effect in the performance of the device.

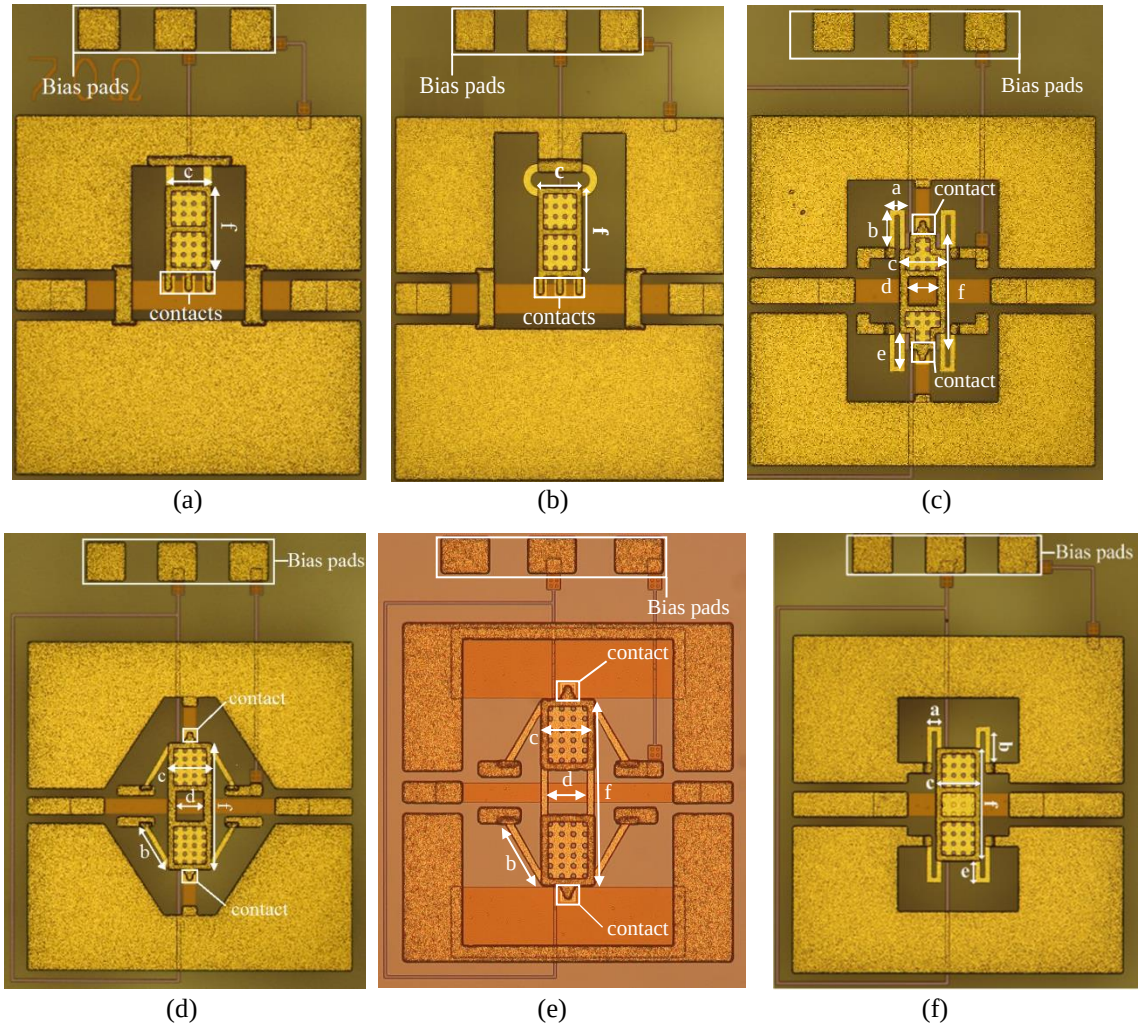

Fig. 9 Fabricated switches on quartz substrate (except (e) on Hi_res Si substrate) in a CPW transmission line structure. Switchable asymmetric shunt impedances: (a) STS cantilever-type ohmic-contact switch. (b) SSS cantilever-type ohmic-contact switch. SABs: (c) FBS bridge-type ohmic-contact switch. (d), (e) DBS bridge-type ohmic-contact switches. (f) FBS bridge-type MIM switched-capacitor.

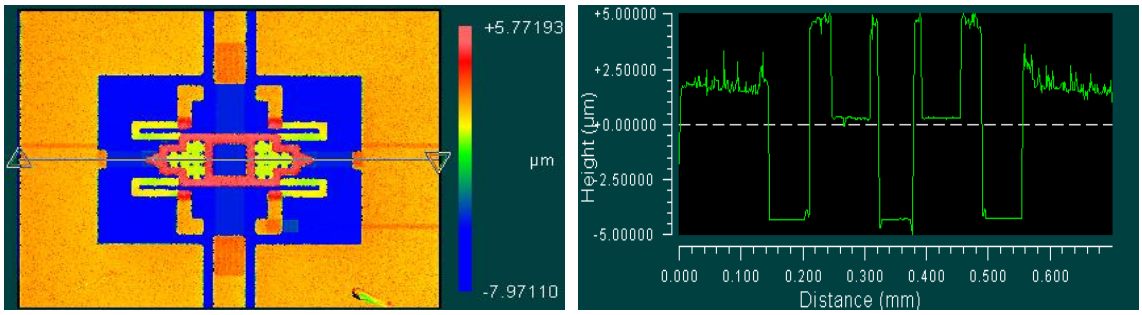

Fig. 10 Optical-profiler measurements of a fabricated ohmic switch

Table 2. Dimensions and simulated mechanical parameters of the switches.

Parameter	STS /SSS ohmic (quartz) g_0: 2.7 μm	FBS ohmic (quartz) g_0: 1.6 / 2.7μm	DBS ohmic (quartz) g_0: 1.6 / 2.7μm	FBS/DBS ohmic (Hi-res Si) g_0: 2.7μm	FBS capacitive (quartz) g_0: 1.6 / 2.7μm
Figure	9(a)/9(b)	9(c)	9(d)	15(b)/9(e)	9(f)
Supporting beam radius (μm)	16				
Meander length, a (μm)		30		30/-	30
Supporting beam width, (μm)	16	10	10	10	10
Supporting beam length, b (μm)	40	75	92	75/107.5	75
Supporting beam length, e (μm)		75	-	25	45
Membrane width, c (μm)	90	90	90	90/90	90
Window width, d (μm)		60	60	60/80	-
Membrane length, f (μm)	170	165	265	230/320	230
Bottom electrodes area (μm^2)	13500	12700	18000	12700/21600	15300
Contact area (μm^2)	10 × 30	10 × 12	10 × 12	10 × 12.3	50 × 90*
Spring constant, k_{eff} (N/m)	2.3 / 1.6	15.4	39.9	14/14	32.5
Pull-in voltage, V_{pull_in} (V)	10.6 / 8.8	12 / 26	16 / 38.2	30 / 30	15.6 / 37.4
Resonant frequency (KHz)	8 / 6.6	17.1	27.3	17	25.3

*MIM area

4. Switch electrical modeling and characterization

In this section the experimental characterization of the fabricated RF-MEMS switches is presented. The switch DC behavior (V_{pull_in} and V_{pull_out}) is derived from measurement of its transmission coefficient (S_{21} parameter) as a function of the applied voltage. This approach has proved to be an adequate and straightforward characterization technique (Contreras et al. 2012). Since the RF-MEMS switches are embedded in CPW transmission structures for characterization and integration purposes, their equivalent circuits take into account the propagating modes which are extracted from the measured S parameters. These models will be used in Section V for the design of reconfigurable multimodal microwave filters in which a full control of the propagating modes is required. The experimental test bench for DC and RF characterization is shown in Fig. 11(a). The DC biasing is performed using an Agilent N6700B power supply. The S parameters are measured with an Agilent PNA-X N5245A network analyzer. Two 150 μm-pitch wafer probes (P1 and P2 in Fig. 11), with either GSG (ground-signal-ground) or SG/GS (signal-ground/ground-signal) configurations are used to contact the RF-MEMS switches. GSG is used to excite the CPW even mode in the capacitive-contact FBS switch and cantilever-type ohmic-contact STS /SSS switches, and SG/GS is used to excite the CPW odd mode in ohmic-contact SAB switches. The photograph of Fig. 11(b) shows the measurement of a (SAB) ohmic switch using SG/GS probes. A third GSG wafer probe (P3) is used to perform the DC contact.

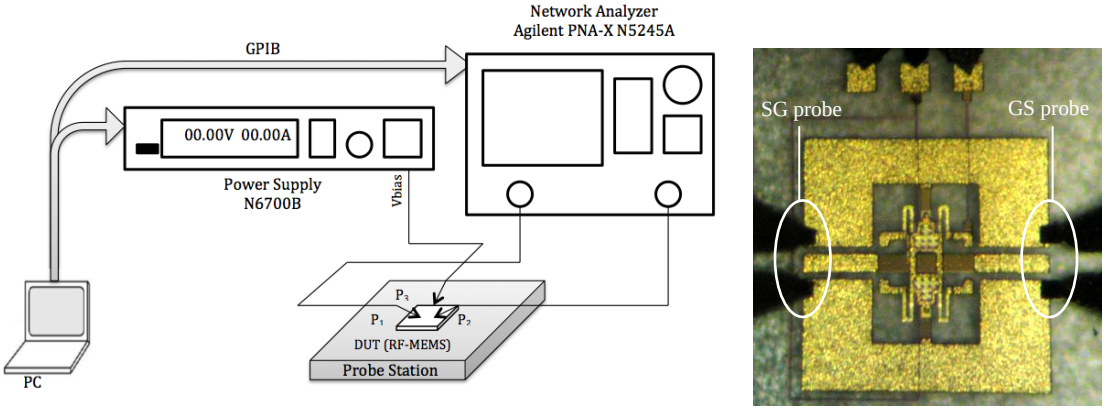

Fig. 11 (a) Experimental test bench for DC and RF characterization. (b) Measurement of the CPW odd-mode switch using SG / GS probes.

Fig. 12 show the hysteresis measurements (magnitude of the transmission coefficient $|S_{21}|$ expressed in dB (i.e. $20\cdot\log(|S_{21}|)$) vs. actuation voltage) of the bridge-type switches shown in Fig. 9, from which the actuation voltages (V_{pull_in}) and the release voltage (V_{pull_out}) can be easily inferred. The measured values for V_{pull_in} are in good agreement with the mechanical simulations presented in Section 3 and are shown in Table 3.

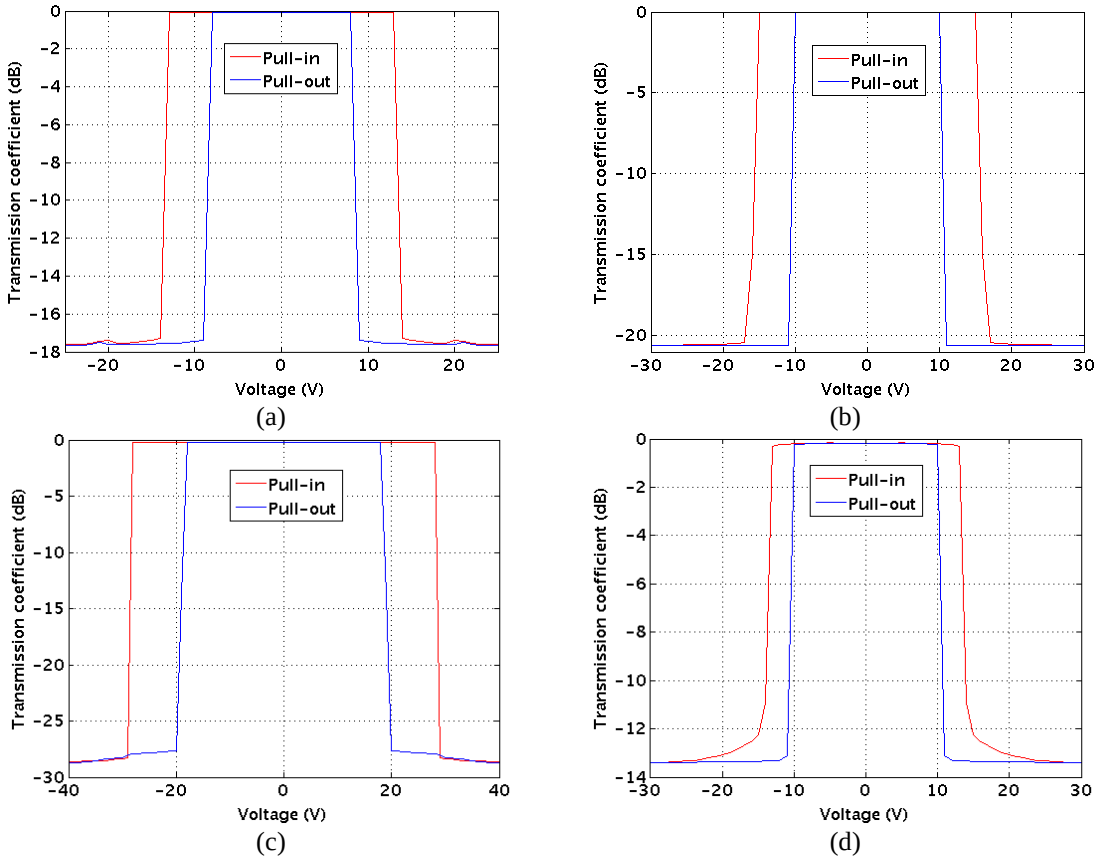

Fig. 12 Hysteresis measurements of the fabricated bridge-type switches. (a) FBS bridge-type ohmic-contact switch (g_0 = 1.6 μm). (b) DBS bridge-type ohmic-contact switch (g_0 = 1.6 μm). (c) DBS bridge-type ohmic-contact switch (g_0 = 2.7 μm). (d) FBS bridge-type capacitive-contact switch (g_0 = 1.6 μm).

Fig. 13 shows the measured transmission coefficient magnitude, $|S_{21}|$ (dB) as a function of the frequency in ON (actuated) and OFF (non-actuated) states. To specify the switch performance, the term *insertion loss* (defined as IL (dB) = –20 log ($|S_{21}|$)), is used in OFF state, while the term *isolation* (also defined as $-20\cdot\log(|S_{21}|)$) is used in ON state. From Fig. 13(a)–(b), the IL of the cantilever-type STS/SSS switches in OFF state for the CPW even mode is IL < 0.9 dB (f < 30 GHz). The STS switch isolation in ON state is higher than 15 dB (f < 7 GHz) and higher than 10 dB (f < 13 GHz). From Fig. 12(c)–(e) the bridge-type FBS/DBS ohmic-contact switches feature IL < 0.9 dB (f < 30 GHz) in OFF state for the CPW odd mode. The switch isolation in ON state is higher than 15 dB (f < 8 GHz) and higher than 10 dB (f < 15 GHz). Therefore, the ohmic-contact switches feature good performances both in the ON and OFF states to implement the intended switchable air-bridge (SAB). As for the capacitive-contact switch (figure 12(f)), it features IL < 0.4 dB (f < 50 GHz) for the CPW even mode in OFF state, and the isolation in ON state is higher than 20 dB (20 GHz < f < 50 GHz). Therefore this switch is well suited for applications in the millimeter-wave frequency range (f > 30 GHz).

Table 3. Measured actuation (V_{pull_in}) and release (V_{pull_out}) voltages (from Fig. 12)

Parameter	V_{pull_in} (V)	V_{pull_out} (V)
FBS ohmic g_0 = 1.6 μm (Fig. 12(a))	13	8.5
DBS ohmic g_0 = 1.6 / 2.7 μm (Fig. 12(b)/(c))	15 / 28	10 / 19
FBS capacitive g_0 = 1.6 μm (Fig. 12(d))	13	10

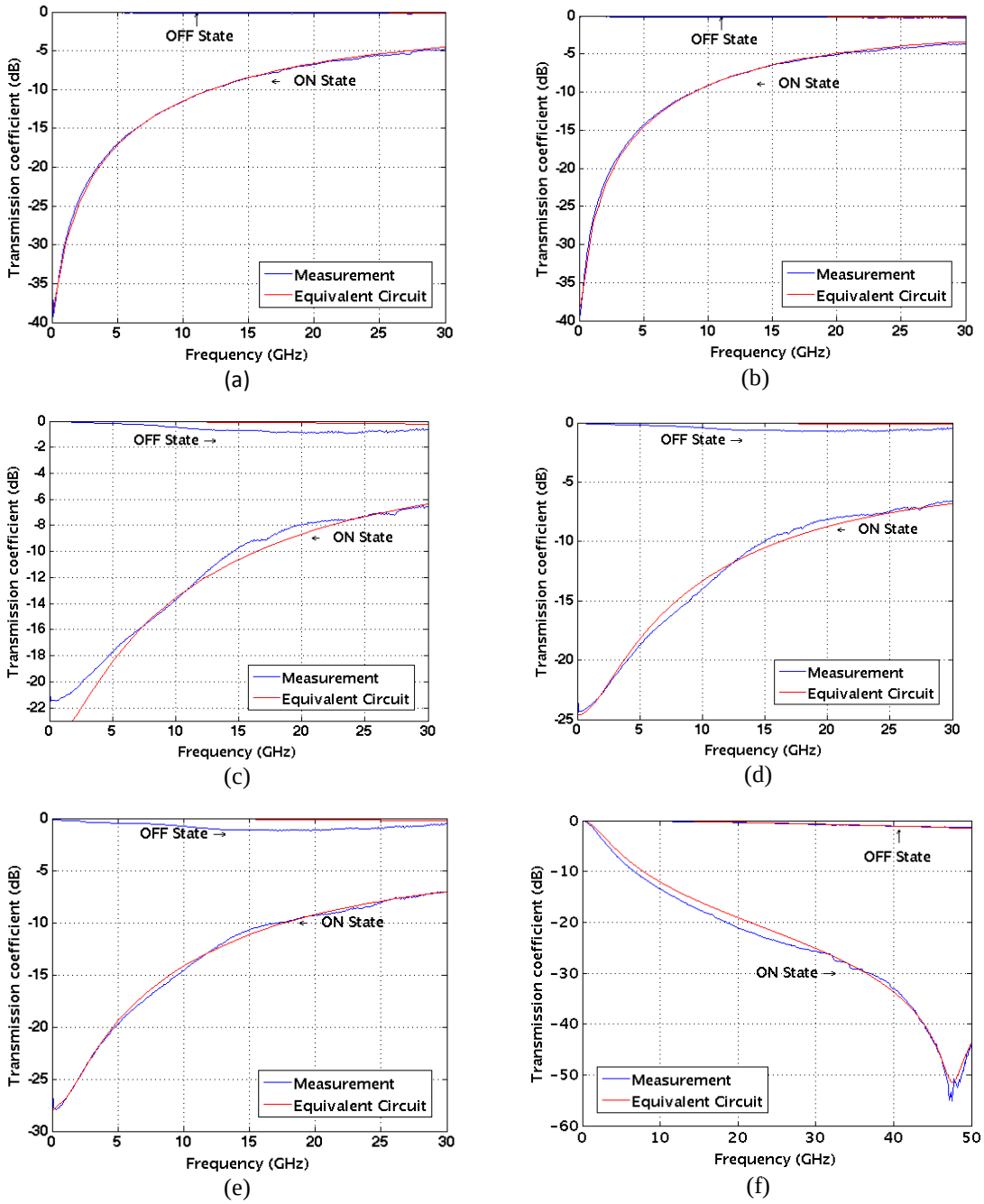

Fig. 13 Measured *S* parameters of the fabricated switches compared to the *S* parameters simulated using the circuit models of Fig. 14. (a) STS cantilever-type ohmic-contact switch. (b) SSS cantilever-type ohmic-contact switch. (c) FBS bridge-type ohmic-contact switch (g_0 = 1.6 μm). (d) DBS bridge-type ohmic-contact switch (g_0 = 1.6 μm). (e) DBS bridge-type ohmic-contact switch (g_0 = 2.7 μm). (f) FBS bridge-type capacitive-contact switch (g_0 = 1.6 μm).

As shown in Fig. 9, the switches are implemented on a CPW test-circuit composed of two CPW sections with different dimensions due to fabrication and measurement constraints. Fig. 14 shows the equivalent

circuit models of the switches. The intrinsic switch behaves as a (shunt-connected) series RL or RLC circuit which is embedded in a structure composed of CPW transmission lines with characteristic impedances corresponding to the odd mode (Z_{0oi}) in case of (SAB) ohmic-contact FBS/DBS switch (Fig. 9(c)–(e), and Fig. 15(b)), or the even mode (Z_{0ei}) in case of capacitive FBS switch (Fig. 9(f)) or cantilever-type STS/SSS switches (Fig. 9(a)–(b)). The inner CPW sections (i = 2) feature wide slots, resulting in a high characteristic impedance than the outer CPW sections (i = 1) with narrow slots (20 μm). The characteristic impedances and propagation constants of each CPW section were obtained from electromagnetic simulation. Small parasitic inductances and capacitances (L_p and C_p, respectively) account for the steps in the width of the CPW lateral ground planes. The values of the circuit elements in Fig. 14 were obtained from the measured S parameters, and are given in Table 4 together with the CPW characteristic impedances.

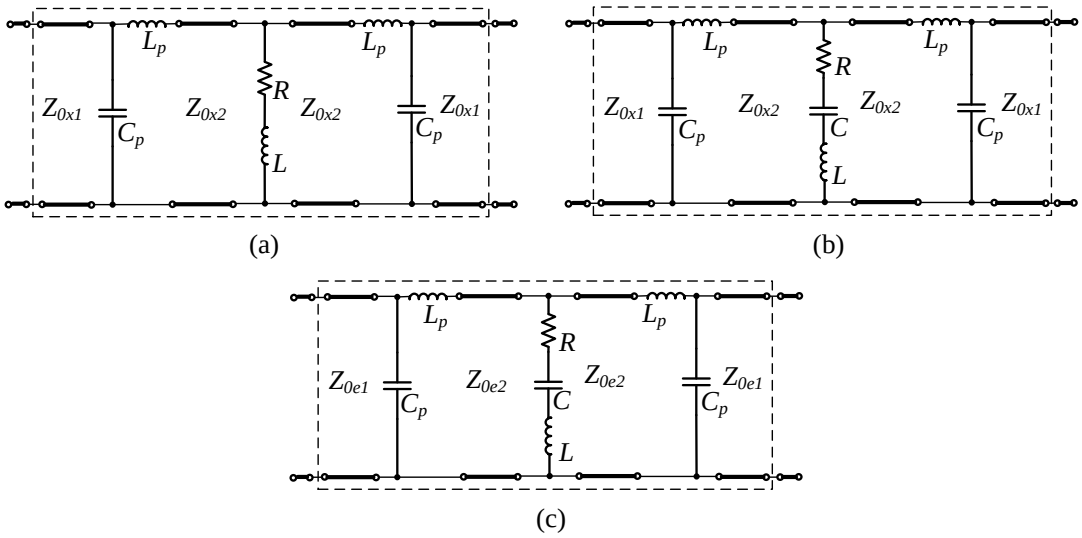

Fig. 14 Equivalent circuit models for the fabricated switches. (a) Ohmic-contact switches in ON state. (b) Ohmic-contact switches in OFF state. (c) Capacitive-contact switches in ON / OFF states. x = e (even) for cantilever ohmic-contact swithes and x = o (odd) for bridge ohmic-contact switch.

The switch inductance L ranges from 0.12 nH to 0.18 nH, and the total resistance (in ON state) R from 1 Ω to 3.2 Ω, including the ohmic-contact resistances. In case of STS and SSS switches, L also includes the even-mode short-ended stub effect of Fig. 2(h). The capacitance of the SAB switches in OFF state is extremely low (C < 1 fF) since the contact area (Table 2) is small. The impact of the SAB switches on the CPW even mode was determined by measuring the switch using GSG probes. The effect is mainly capacitive (an even-mode capacitance C_{even}). The window opened in the membrane minimizes the overlapping area between bridge and CPW central conductor, resulting in a small capacitance value, which is minimized in the Hi-res Si substrate switch (C_{even} = 47 fF) with larger window with respect to the quartz substrate switch (C_{even} = 95 fF). Regarding the capacitive-contact switch, its circuit model is composed by a series RLC circuit shunt-connected to the CPW even-mode transmission line for both (ON and OFF) states (Fig. 14(c)). The switch capacitance value is very small in OFF state (C_{OFF} = 32 fF) and a very high in ON state (C_{ON} = 1.53 pF). Thus the capacitance ratio is very high (C_{ON} / C_{OFF} = 47.8). The switch resistance and inductance are also very small (L = 7 pH and R = 0.1 Ω). Therefore, a very high series-resonance frequency is obtained (48.6 GHz), which agrees with the measured isolation peak in Fig. 13(f). A good agreement between the electrical circuit model and the measurements is obtained, thus validating the circuit models of Fig. 14 for design purposes.

Table 4. Equivalent circuit elements of Fig. 13.

Parameter	STS / SSS		FBS (quartz) ohmic switch		DBS (quartz) ohmic switch		FBS (*Hi_res Si*) ohmic switch		DBS (*Hi_res Si*) ohmic switch		FBS (quartz) capacitive switch	
	OFF	ON	OFF	ON	OFF	ON	OFF	ON	OFF	ON	OFF	ON
L_p (*nH*)	0.02		0		0.045		0		0		0	
C_p (*fF*)	0		3		6.5		6		6		8.5	
L(*nH*)	0.1	0.1	0.18	0.18	0.18	0.18	0.12	0.12	0.12	0.12	0.007	0.007
C (*fF*)	5.1	–	0.9	–	0.5	–	1	–	1	–	32	1530
R (Ω)	0	1	0.3	3.2	0.3	3	0.3	1.5	0.3	1.5	0.1	0.1
Z_{0x1} (Ω) *	45.3		101.7		96.3		78.1		72.1		78.6	
Z_{0x2} (Ω) *	63.5		199.1		200.3		126.7		143.5		148.5	

*x = e (even) or o (odd) according to Fig. 14

5. Design of multimodal microwave reconfigurable filters

In this last section, application examples of the switches proposed and implemented in the preceding sections will be presented to highlight their use to selectively control the propagating modes, thus enabling reconfiguration in compact microwave multimodal bandpass filters. A first example is shown in Fig. 15(a) (Contreras et al. 2014). The filter was fabricated on a 5-kΩ·cm Hi_res silicon substrate and is composed of two $\lambda_o/4$ slotline resonators, coupled using a slotline gap. Each resonator is fed by a reconfigurable multimodal immitance inverter structure (MIIs K_{01} and K_{23}) (Contreras et al. 2013) which multimodal equivalent circuit can be easily inferred from Fig. 3 and is shown in Fig. 15(c). The length of each resonator is controlled by a SAB (Fig. 15(b)) which, when actuated, reduces the resonator effective length. This length shift increases in turn the resonators' resonance frequency and therefore the filter center frequency is shifted up. The filter features two frequency states at 12 GHz and 13 GHz, respectively, with a constant fractional bandwidth (FBW) of 14%. To accurately simulate the filter response, the equivalent circuit of Fig. 14(a)–(b) is used as SAB element in Fig. 15(c). Note that the multimodal approach, besides transferring energy from the exciting even mode to the resonant odd mode, allows filter reconfiguration and embedding the MIIs within the resonators, thus saving circuit area. Fig. 15(d) compares the filter measured *S* parameters with simulations, showing a good agreement. The filter IL is 4.6 dB in both states.

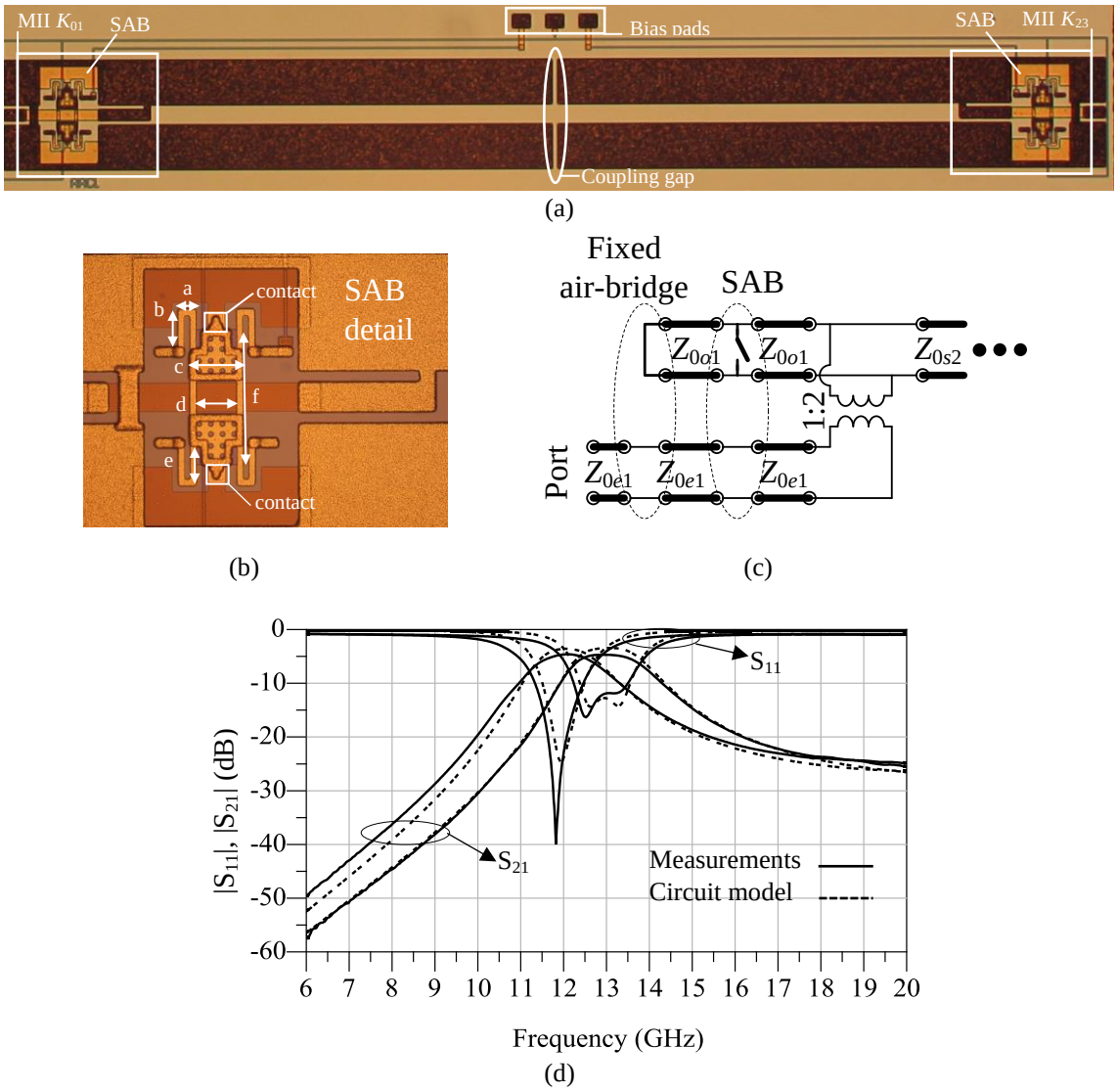

Fig. 15 Multimodal bandpass filter with capacitively-coupled slotline resonators whose center frequency is controlled by SABs (Contreras et al. 2014). (a) Fabricated filter on a High-res Si substrate. (b) Detail of the switch. (c) Multimodal model of one MII and detail of the embedded SAB. (d) Measured filter *S* parameters for the two states compared to those predicted by its multimodal circuit model.

A second example is shown in Fig. 16(a) (Contreras et al. 2013). The filter was fabricated on a quartz substrate and is composed of two $\lambda_o/2$ slotline resonators, coupled using an impedance inverter, K_{12} (slotline short). Each resonator is fed by a reconfigurable MII (K_{01} and K_{23}), which multimodal equivalent circuit inferred from Fig. 3 is shown in Fig. 16(b). Now the resonator length is kept constant (fixed air-bridge) and the position of the asymmetric short circuit is changed instead. This results in filter FBW reconfiguration with constant center frequency (Contreras et al. 2013). To modify the asymmetric short circuit position, each MII integrates two switchable asymmetric shunt impedances (short-circuits) as those explained in Section II (Fig. 2(g)), here implemented using cantilever STS switches placed in one of the CPW slots (Fig. 16(c)). When actuated, these switches modify the filter inverters K_{01} and K_{23} (and transfer energy from the exciting even mode to the resonant odd mode), resulting in a change in the filter fractional bandwidth (FBW). To keep the central frequency constant, another cantilever STS switch is integrated in K_{12} and actuated simultaneously. The filter features two FBW states (0.082 when the inner switches are actuated and 0.044 when the outer switches and the impedance inverter switch are actuated, respectively) while maintaining a constant filter center frequency (18.9 GHz) and same response. Fig. 16(d) compares the filter measured *S* parameters with simulations, showing a good agreement.

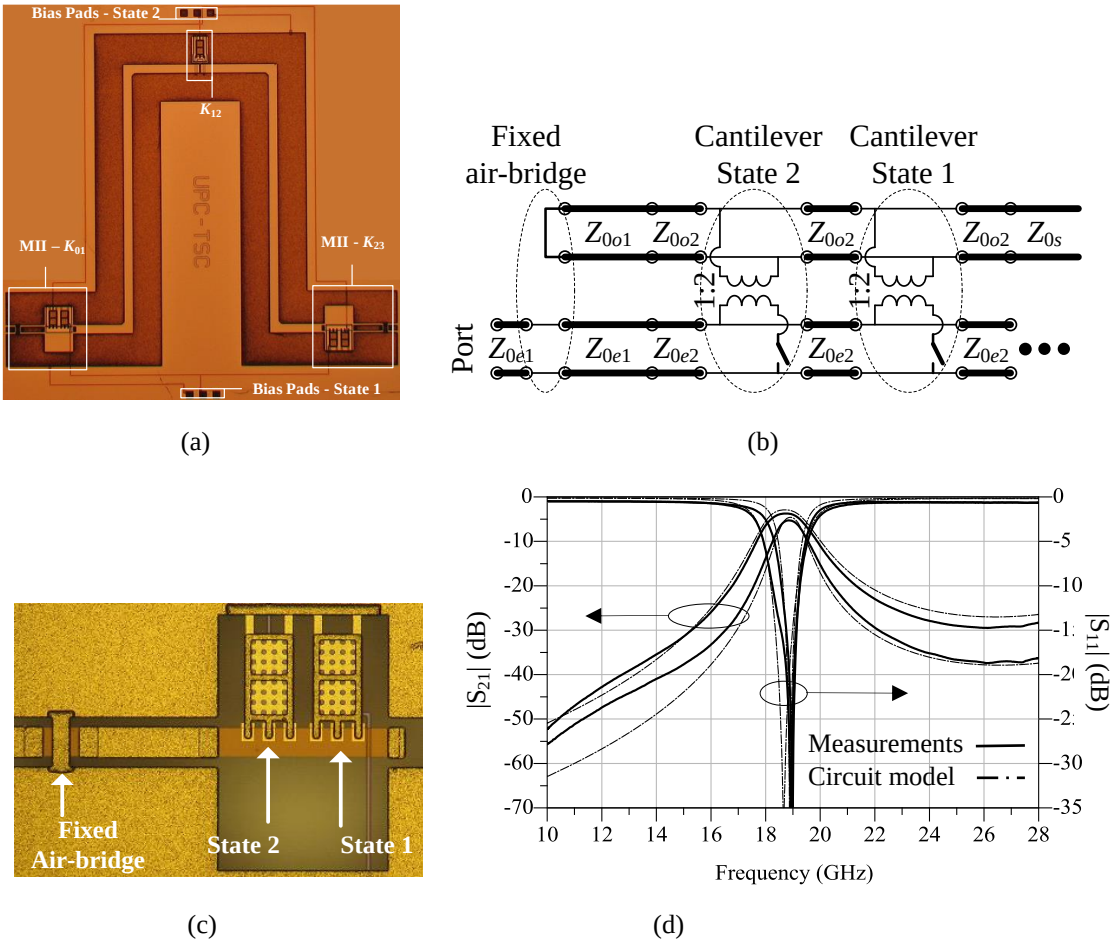

Fig. 16 Multimodal bandpass filter with inductively-coupled slotline resonators which fractional bandwidth is controlled by switchable asymmetric shunt short-circuits (two cantilever STS switches per resonator) (Contreras et al. 2013). (a) Fabricated filter on quartz substrate. (b) Multimodal model of one MII (c) Detail of the STS switches. (d) Measured filter *S* parameters for the two states compared to those predicted by its multimodal circuit model.

6. Conclusions

In this paper, new RF-MEMS switch configurations required to control the even and odd propagating modes in multimodal CPW transmission structures have been identified and studied in detail. Specifically a *switchable air-bridge* (SAB) using a new class of bridge-type switch with a double ohmic-contact, and a *switchable asymmetric shunt impedance* using a cantilever-type switch with a single ohmic-contact, have been proposed and implemented. In either case, different optimized-shape suspension configurations have been used to enhance (in combination with a reinforced membrane) the structure robustness against fabrication stress gradients. The switches have been exhaustively modelled using a coupled-field 3D finite-element mechanical analysis. Simulations show that the bridge-type switches exhibit higher stiffness constant than cantilever-type, with a moderate pull-in voltage (15 V for an electrode gap of 1.6 μm). The DBS bridge-type switches have shown a similar initial deformation but an increased contact force compared to FBS (with equal beam-length suspensions). The switches have been fabricated using the eight-mask surface-micromachining RF-MEMS process from FBK and have been extensively characterized. The actuation and release voltages have been derived from hysteresis measurements of the magnitude of the transmission coefficient, $|S_{21}|$, at microwave frequencies. The actuation voltages are in good agreement with the simulated values. From the *S*-parameter measurements, an electrical model has been obtained for the switches in ON and OFF states, showing a very good agreement with the measurements. The electrical circuit model has been successfully applied to the design of compact reconfigurable multimodal microwave bandpass filters wherein either the center frequency or the fractional bandwidth can be reconfigured.

Acknowledgements

This work has been funded by research project TEC2013-48102-C2-1/2-P and fellowship BES-2008-004923 from the Spanish Ministry of Economy and Competitiveness, and fellowships 340469 and 410742 from the Mexican CONACYT.

6. References

Contreras A, Casals-Terré J, Pradell L, Giacomozzi F, Iannacci J and Ribó M (2014) A Ku-band RF-MEMS frequency-reconfigurable multimodal bandpass filter Int. J. Microw. Wireless Tech. **6** :277–85 doi: 10.1017/S1759078714000567

Contreras A, Casals-Terré J, Pradell L, Giacomozzi F, Colpo S, Iannacci J and Ribó M (2012) A RF-MEMS switchable CPW air-bridge In: 7th European Microwave Integrated Circuits Conference, Amsterdam, 2012 :441–444

Contreras A, Pradell L, Ribó M (2011) A Novel Tunable Multimodal Bandpass Filter (2011) In: 41st European Microwave Conference EuMC-2011, Manchester- UK, 2011:1059-1062

Contreras A, Ribo M, Pradell L, Blondy P (2013) Uniplanar bandpass filters based on multimodal immitance inverters and end-coupled slotline resonators. IEEE transactions on microwave theory and techniques, 61(1):77-88 doi:10.1109/TMTT.2012.2226743

Contreras A, Ribó M, Pradell L, Casals-Terré J, Giacomozzi F and Iannacci J (2013) K-band RF-MEMS uniplanar reconfigurable-bandwidth bandpass filter using multimodal immittance inverters Electron. Lett. **49** :704–706 doi: 10.1049/el.2013.0681

Entesari K and Rebeiz G M (2005) A differential 4-bit 6.5-10-GHz RF MEMS tunable filter IEEE Trans. on Microw. Theory Tech. **53** :1103–1110 doi: 10.1109/TMTT.2005.843501

Fedder G K (1994) Simulation of microelectromechanical systems PhD Thesis Dept. EECS University of California, Berkeley, USA

Fourn E, Pothier A, Champeaux C, Tristant P, Catherinot A, Blondy P, Tanne G, Rius E, Person C and Huret F (2003) MEMS switchable interdigital coplanar filter IEEE Trans. on Microw. Theory Tech. **51** :320–324 doi: 10.1109/TMTT.2002.806517

Giacomozzi F, Mulloni V, Colpo S, Iannacci J, Margesin B and Faes A (2011) A flexible fabrication process for RF MEMS devices Romanian J. of Inform. Science and Tech. **14** :259–268

Ke F, Miao J and Oberhammer J (2013) A ruthenium-based multimetal-contact RF MEMS switch with a corrugated diaphragm J. Micromech. Syst. **22** :1447–1459 doi: 10.1109/JMEMS.2008.2004786

Kim J, Kwon S, Jeong H, Hong Y, Lee S, Song I, Ju B (2009) A stiff and flat membrane operated DC contact type RF MEMS switch with low actuation voltage. Sensors and Actuators A: Physical **153** :114-119 doi: 10.1016/j.sna.2009.04.002

Kim M, Song Y, Ko S, Ahn S, Yoon J (2014) Ultra-low voltage MEMS switch using a folded hinge structure. Micro and Nano Systems Letters **2** 2 doi: 10.1186/s40486-014-0002-y

Lakshmi S · Manohar P · Sayanu N (2016) Optimization of structures of DC RF MEMS series switches for low actuation Microsyst Technol. doi:10.1007/s00542-016-3063-4

Lucyszyn S (2004) Review of radio frequency microelectromechanical systems technology Science, Meas. and Tech., IEE Proc. **151 :**93–103 doi: 10.1049/ip-smt:20040405

Llamas M A, Ribó M, Girbau D, Pradell L (2009) A Rigorous Multimodal Analysis and Design Procedure of a Uniplanar 180º Hybrid IEEE Trans. on Microw Theory Tech. 57 :1832 – 1839 doi: 10.1109/TMTT.2009.2022881

Llamas M A, Girbau D, Ribó M, Pradell L, Giacomozzi F and Colpo S (2011) RF-MEMS uniplanar 180º phase switch based on a multimodal air-bridged CPW cross IEEE Trans. on Microw Theory Tech. **59** :1769–1777 doi: 10.1109/TMTT.2011.2140125

Llamas M A, Girbau D, Ribó M, Pradell L, Lázaro A, Giacomozzi F and Margesin B (2010) MEMS-based 180° phase switch for differential radiometers IEEE Trans. on Microw Theory Tech. **58 :**1264–1272 doi: 10.1109/TMTT.2010.2045558

Mahameed R and Rebeiz G M (2010) A high-power temperature-stable electrostatic RF MEMS capacitive switch based on a thermal buckle-beam design J. Micromech. Syst. **19** :816–826 doi: 10.1109/JMEMS.2010.2049475

Mulloni V, Colpo S, Faes A and Margesin B (2013) A simple analytical method for residual stress measurement on suspended MEM structures using surface profilometry J. Micromech. Microeng. **23** doi: 10.1088/0960-1317/23/2/025025

Nadaud K,Roubeau F, Zhang L-Y, Stefanini R, Pothier A, and Blondy P, (2016) Compact thin-film packaged RF-MEMS switched capacitors, in International Microwave Symposium, (San Francisco USA) doi: 10.1109/MWSYM.2016.7540062

Nordquist C D, Goldsmith C L, Dyck C W, Kraus G M, Finnegan P S, Austin F and Sullivan C T (2005) X-band RF MEMS tuned combline filter Electron. Lett. 41 :76–77 doi: 10.1049/el:20057375

Nordquist C D, Muyshondt A, Pack M V, Finnegan P S, Dyck C W, Reines I, Kraus G M, Plut T A, Sloan G R, Goldsmith C L and Sullivan T (2004) An X-band to Ku-band RF MEMS switched coplanar strip filter IEEE Microw. Wireless Comp. Lett. **14** :425–427 doi: 10.1109/LMWC.2004.832071

Ocera A, Farinelli P, Mezzanotte P, Sorrentino R, Margesin B and Giacomozzi F (2006) A novel MEMS-tunable hairpin line filter on silicon substrate Proc. 36th European Microwave Conf. (Manchester) :803–806 doi: 10.1109/EUMC.2006.281041

Palego C, Deng J, Peng Z, Halder S, Hwang J C M, Forehand D I, Scarbrough D, Goldsmith C L, Johnston I, Sampath S K and Datta A (2009) Robustness of RF MEMS capacitive switches with molybdenum membranes IEEE Trans. on Microw Theory Tech. **57** :3262–3269 doi: 10.1109/TMTT.2009.2033885

Park S J, Lee K Y and Rebeiz G (2006) Low-loss 5.15–5.70-GHz RF MEMS switchable filter for wireless LAN applications IEEE Trans. on Microw. Theory Tech. **54** :3931–3939 doi: 10.1109/TMTT.2006.884625

Patel C D and Rebeiz G M (2012) A high-reliability high-linearity high-power RF-MEMS metal-contact switch for DC–40-GHz applications IEEE Trans. on Microw Theory Tech. **60** :3096–3112 doi: 10.1109/TMTT.2012.2211888

Peroulis D, Pacheco S P, Sarabandi K and Katehi L P B (2003) Electromechanical considerations in developing low-voltage RF MEMS switches IEEE Trans. on Microw Theory Tech. **51** :259–270 doi: 10.1109/TMTT.2002.806514

Persano A, Quaranta F, Capoccia G. Siciliano P. (2016) Influence of design and fabrication on RF performance of capacitive RF MEMS switches Microsyst Technol **22** :1741-1746 doi:10.1007/s00542-016-2829-z

Philippine M A, Sigmund O, Rebeiz G M and Kenny T W (2013) Topology optimization of stressed capacitive RF MEMS switches J. Micromech. Syst. **22** :206–215 doi: 10.1109/JMEMS.2012.2224640

Pothier A, Orlianges J C, Guizhen Z, Champeaux C, Catherinot A, Cros D, Blondy P and Papapolymerou J (2005) Low-loss 2-bit tunable bandpass filters using MEMS DC contact switches IEEE Trans. on Microw. Theory Tech. **53** :354–360 doi: 10.1109/TMTT.2004.839935

Rebeiz G, Entesari K, Reines I, Park S J, El-tanani M, Grichener A and Brown A (2009) Tuning in to RF MEMS IEEE Microwave Magazine **10 :**55–72 doi: 10.1109/MMM.2009.933592

Reines I, Brown A, El-Tanani M, Grichener A and Rebeiz G (2008) 1.6-2.4 GHz RF MEMS tunable 3-pole suspended combline filter Proc. IEEE MTT-S Int. Microwave Symp. (Atlanta) :133–136 doi: 10.1109/MWSYM.2008.4633121

Ribó M and Pradell L (1999) Circuit model for mode conversion in coplanar waveguide asymmetric shunt impedances Electronics Letters. **35** :713–715 doi: 10.1049/el:19990507

Scarbrough D, Goldsmith C, Papapolymerou J and Li Y (2009 Miniature microwave RF MEMS tunable waveguide filter Proc. 39th European Microwave Conf. (Rome) :1860–1863

Sterner M and Oberhammer J (2008) Symmetrical antidirectional metallization for stress compensation of transfer-bonded monocrystalline silicon membranes J. Micromech. Syst. **17** :195–205 doi: 10.1109/JMEMS.2012.2224642

Van Caekenberghe K and Vaha-Heikkila T (2008) An analog RF MEMS slotline true-time-delay phase shifter IEEE Trans. on Microw. Theory Tech. **56** :2151–219 doi: 10.1109/TMTT.2008.2002236

Wolff I (2006) Coplanar microwave integrated circuits John Wiley & Sons, Inc, Hoboken, New Jersey.

Wong W C, Azid I A, and Majlis B Y (2011) Theoretical analysis of stiffness constant and effective mass for a round-folded beam in MEMS accelerometer J. of Mech. Engineering 57 :517–525 doi: 10.5545/sv-jme.2009.151

Yang H, Zareie H, and Rebeiz G, Fellow (2015) High Power Stress-Gradient Resilient RF MEMS Capacitive Switch J. Micromech. Syst. 24-3 doi: 10.1109/JMEMS.2014.2335173

Young W C, Budynas R G and Sadegh A M (2012) Roak's Formulas for Stress and Strain, 8th ed. (New York: McGraw-Hill)

Yuk K Y, Fouladi S, Ramer R and Mansour R R (2012) RF MEMS switchable interdigital bandpass filter IEEE Microw. Wireless Comp. Lett **22** :44–46 doi: 10.1109/LMWC.2011.2176926

Zareie H and Rebeiz G M (2013) High-power RF MEMS switched capacitors using a thick metal process IEEE Trans. on Microw Theory Tech. **61** :455–463 doi: 10.1109/TMTT.2012.2226744